2D Hybrid Germanium Iodide Perovskites

Despoina Manidaki

February 2022

Department of Materials Science and Technology

University of Crete

PREFACE

This work was completed in the field of inorganic chemistry, specifically in the crystal chemistry laboratory of the University of Crete's Department of Materials Science and Technology, under the supervision of Professor Constantinos C. Stoumpos, whom I would like to thank for all the valuable knowledge and helpful assistance he provided me in this type of materials, the Perovskites, which I was unfamiliar with at the time. I'd also like to thank the entire research team for their assistance in getting me started and giving me with important information during the study process. As well as PhD and postgraduate students, who assisted me in taking sample characterization measures and taught me how to use the laboratory equipment.

Contents

1. Introduction

1.1 General Aspects of the Perovskites

The calcium titanium oxide mineral of chemical formula $CaTiO_3$, was discovered in 1839 by the Prussian mineralogist Gustav Rose in mineral deposits in the Ural Mountains. The name given to this mineral, is Perovskite in honor of the Russian mineralogist Count Lev Alexevich von Perovski. From the hundreds of compounds known to adopt the Perovskite structure, the mineral Bridgmanite $(Fe, Mg)SiO_3$ is found in greater abundance in heartland of the earth and accounts for 38% of the total.[1]

Nowadays, the name perovskite is used for a large family of compounds that has the general chemical formula ABX_3. Positions A and B consist of metal ions with the former being larger than the latter ($r_A > r_B$), while the X position is usually occupied by a chalcogen or halogen anion. To produce a stable perovskite structure, the cations must simply rest on the surrounding anions, according to Goldschmidt's rule. That is, it is defined by the following relationship:

$$t = \frac{(r_A + r_X)}{\sqrt{2}(r_B + r_X)} = 1 \text{ (ideal structure)}$$

, here *t* is the tolerance factor and indicates that a perovskite must have a value near to 1 in order to form. The radius of the cation situated outside the octahedron, i.e. at the cage's vertices, is r_A. The radius of cation B, which is positioned in the octahedron's center and related to the six anions, is r_B. The radius of the anion is r_X. Because the ionic radii of perovskite structures containing oxides are better defined and are more precisely known, the tolerance factor has higher significance and predictive power.

The ideal cubic perovskite structure is obtained when t is between 0.9 and 1. If t > 1, which indicates that cation A is large and cation B is small, hexagonal structures (polytypes) of AMX_3 chains form with a $BaNiO_3$ structure-type. When t is between 0.71 and 0.9, the octahedral lattice is distorted, resulting in a crystal structure with lower symmetry than the cubic. When the value of t is even smaller, i.e. the cations A and B become similar in size, structures like ilmenite, $FeTiO_3$, or the rare earth type cubic structure Ln_2O_3 (bixbyite) form.

The compounds with formula ABO_3 are the ionic ceramic perovskites. The usefulness of the physical and chemical properties of these materials is very important for many industrial and technological applications such as dielectrics, ferroelectrics and superconductors. [1,2 3]

One of the oldest technologically relevant material is $BaTiO_3$. As one proceeds from high to low temperatures, the structure of $BaTiO_3$ changes due to deformation of the TiO_6 octahedra, as shown in **Figure 1** below. The material's ferroelectric nature changes substantially at T_c = 120 ^{0}C, when it undergoes a phase transition from a non-polar,

centrosymmetric (cubic) lattice to a polar non-centrosymmetric (tetragonal) lattice, thus creating an uncompensated permanent dipole moment.

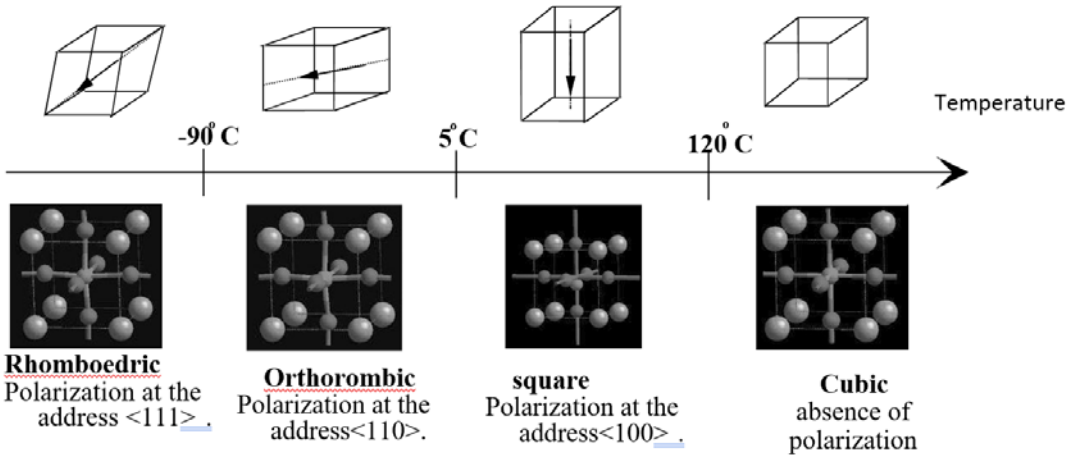

Figure 1: The crystal structure of $BaTiO_3$ changes with temperature.

In addition to oxygen perovskites, the class of halide perovskite compounds of the chemical formula AMX_3 (A = Cs^+, $CH_3NH_3^+$, or $HC(NH_2)^{2+}$, M = Ge^{2+}, Sn^{2+}, Pb^{2+}, X = Cl^-, Br^-, I^-) has been studied and synthesized in recent years, due to significant achievements in the field of photovoltaics,[4-12] tarting with the compound $CH_3NH_3PbI_3$ which was used as a light absorber in solar cells with significant efficiency at the end of 2012.[13-15] Despite the excellent power conversion efficiency of the solar cells that use these materials, they have two major drawbacks. The first is that there is long-term instability in the devices that use these materials and the second is that there is a high degree of toxicity, due to the presence of the lead element.[16-17]

Thus, the replacement of lead (Pb) with metals such as tin (Sn) and germanium (Ge), which have a much lower toxicity content, can be applied to the manufacture of environmentally friendly devices.[18-23] Also, the problem of instability could be addressed by the formation of two-dimensional (2D) layered iodide perovskites, which arise during the slicing of three-dimensional (3D) corresponding frameworks into 2D slabs.[24,25] On this occasion, in the context of the present work, the aim was the synthesis and characterization of 2D hybrid iodine perovskites based on germanium. Apart from its low toxicity, germanium was chosen as the metal of the perovskites because it exhibits a very strong second harmonic generation (SHG) response, which is attributed to the high density of states in the valence band due to sp hybridization of the orbitals Ge and I because of lone pair activation, according to first principles calculations of the electronic structure using density functional density theory.[26] The absence of a crystallographic center of inversion in the structure is required for the formation of this feature, which applies to two-dimensional structures of perovskite with germanium.[27] This is because the chemical element Ge is small in size and thus, to stabilize the octahedral structure formed through the bonds of germanium with six iodines, displaces off-center. Thus, the octahedron is deformed, and its angles deviate from 90 degrees, as well as the bonds are not all equal to each other, resulting in a complete bipolar moment and therefore the SHG effect.

1.2 General Aspects of the Perovskites

The second-harmonic generation is a nonlinear process in which two photons of the same frequency interact with a nonlinear material, combining to form a new photon with twice the energy, twice the frequency, and half the wavelength of the original photons.[28] Coherent light can be produced by materials with this feature at variable frequencies. This property can thus be applied to the manufacturing and engineering of lasers, as well as the imaging of living cells in the biosciences, telecommunications, and military applications.

The equation describes the relationship between the material's non-linear polarization and the electric field is: [28]

$$\begin{aligned} P^{\text{nonlinear}} &= \epsilon_0 \chi^{\text{nonlinear}} \mathcal{E} \\ &= \epsilon_0 \chi^{(1)} \mathcal{E} + \epsilon_0 \chi^{(2)} \mathcal{E}^2 + \epsilon_0 \chi^{(3)} \mathcal{E}^3 + \cdots \end{aligned}$$

, where ε is the magnitude of the applied field.The dielectric constant depends on the electric field through the nonlinear sensitivities (susceptibilities?), according to the relation:

$$\begin{aligned} \epsilon_{\text{r}}^{\text{nonlinear}} &= 1 + \chi^{\text{nonlinear}} , \\ &= 1 + \chi^{(1)} + \chi^{(2)} \mathcal{E} + \chi^{(3)} \mathcal{E}^2 + \cdots \end{aligned}$$

[28]The anisotropic nonlinear response of the medium for the second order nonlinear polarization $P^{(2)}$ is described according to the relation:

$$P_i^{(2)} = \epsilon_0 \sum_{j,k} \chi_{ijk}^{(2)} \mathcal{E}_j \mathcal{E}_k \, .$$

$\chi^{(2)}$ijk is the second-order nonlinear susceptibility tensor and i, j, k are the Cartesian x,y and z axes.

1.3 The perovskite crystal structure

The ideal unit cell of the crystal structure of ABX_3 perovskites is cubic, where the cations A are coordinated to 12 anions X and the cations B are coordinated to 6 anions X. The latter make bonds with two cations B and 4 cations A. An example of a compound showing this structure at room temperature is $SrTiO_3$, with crystal lattice parameter a = 0.3905 nm and space group $Pm\bar{3}m$(**Figure 2**). [1]

The atoms can be placed in the building unit in two different ways, resulting in the creation of two different unit cell arrangements[1]. In the first case, which is the typical crystallographic arrangement, the large cations $Sr^{2+}$are placed at the corners of the unit cell and the smaller cations Ti^{4+} in the center, which are surrounded by the six anions O^{2-} to form octahedrons TiO_6 (picture 2). Specifically, the atomic coordinates of this structure are a) Sr (1) 0,0,0, b) Ti (1) ½, ½, ½, c) O (3) ½, ½, 0; ½, 0, ½; 0, ½, ½.

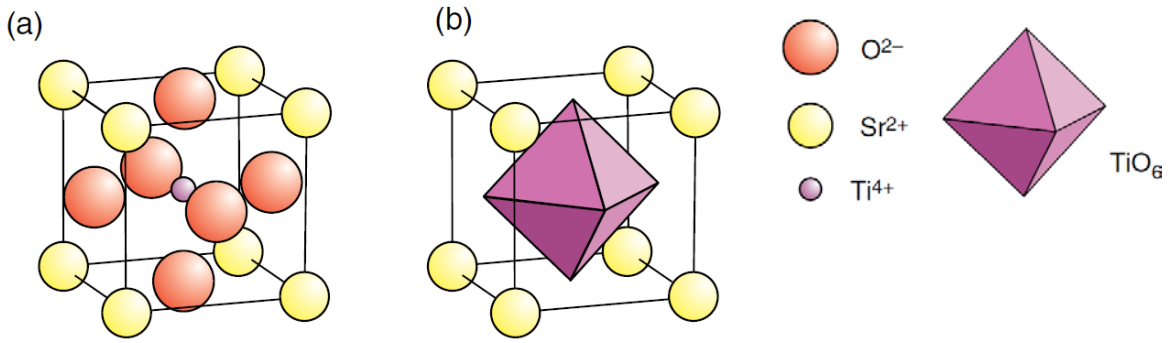

Figure 2: The idealized perovskite structure of $SrTiO_3$: (a) atom positions with Sr^{2+} at cell origin; (b) TiO_6 octahedral coordination polyhedron.

The second case is mainly used to facilitate the study of the chemical and physical properties of perovskites.[1] The cations Sr^{2+} are now placed in the center of the unit cell and surrounded by oxygen ions O^{2-} cuboctahedral (**Figure 3**). So, the positions of the atoms in the cell will now be a) Ti (1) 0,0,0, b) Sr (1) ½, ½, ½, c) O (3) ½, 0, 0; 0, ½ ,0; 0, 0, ½. In the ideal structure, octahedrons have all the bond lengths Ti^{4+}-O^{2-} equal. Additionally, the six bonds O^{2-} Ti^{4+}-O^{2-} are linear.

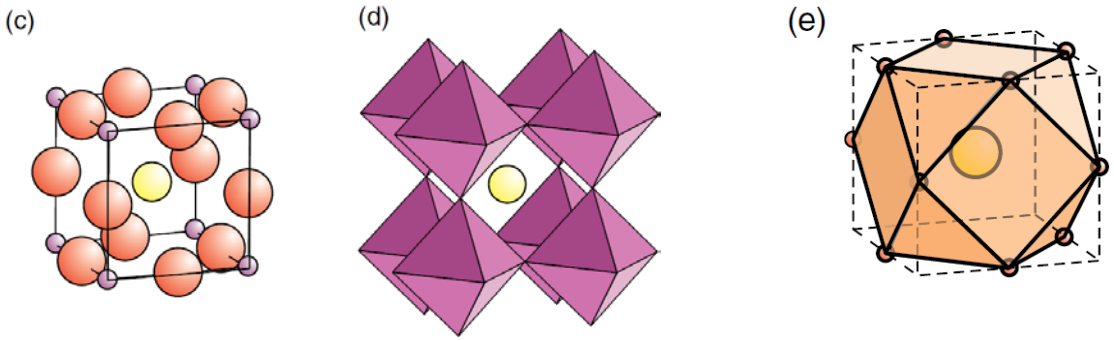

Figure 3: (c) atom positions with Ti^{4+} at cell origin; (d) TiO_6 octahedral polyhedron framework with Sr^{2}+ at the cell centre; (e) cuboctahedral cage site.

[26]The elementary structural unit, namely the unit cell, is repeated periodically in space and finally the three-dimensional (3D) crystal framework of the perovskite is created, which is assembled through singe B-X-B bridges to form $[BX_6]^{4-}$ corner-sharing octahedra. The A cations are included between the cavities formed by these frameworks of octahedra.

1.4 Hybrid organic-inorganic two-dimensional perovskites

The general chemical formula for reduced dimension perovskites, specifically two dimensional (2D), is $(RNH_3)_2(A)_{n-1}MX_{3n+1}$. The principal aliphatic or aromatic alkylammonium cation that acts as a spacer between the perovskite layers is referred to as RNH_3. While term A is a smaller organic alkylammonium cation than term RNH_3, it is found inside the cavities generated by the corner-sharing octahedra, just like in 3D structures. The cations A, M, and anions X are the building blocks that make up the perovskite framework. That is, inorganic perovskite layers are formed from $[MX_6]^{4-}$octahedrons joined through their corners and separated by bilayers of massive organic alkylammonium cations. In this way the 2D network is formed.[29] The semiconducting inorganic perovskite layers act as wells, and the insulating organic layers act as barriers, forming natural multiple configurations of quantum wells.[30,31] Due to the low dimension and dielectric characteristics difference between the organic spacers and the inorganic perovskite layers, these compounds produce stable excitons with high binding energy at ambient temperature.[32] 2D perovskites are utilized in optical and electronic applications like field-effect transistors (FETs), light-emitting diodes (LEDs), and hard radiation detectors because of this.[32-34]

Although several two-dimensional perovskites including Pb and Sn have been synthesized and characterized, as shown in the following examples, $(BA)_2(MA)_{n-1}Pb_nI_{3n+1}$ (n=2-5)(BA=butylammonium),[35,36] and $(BA)_2(MA)_{n-1}Sn_nI_{3n+1}$ (n=2-3)[37,38] very little mention has been made of the 2D organic-inorganic perovskites with Ge (II), mainly the n = 1 $(C_4H_9NH_3)_2GeI_4$ member. This could be because Ge's divalent state is more unstable than the metals Pb and Sn in the group 14 of the periodic table.[39]

The synthesis, crystal structure description, and optical properties of the homologous 2D series of germanium iodide perovskites $(CH_3(CH_2)_3NH_3)_2(CH_3NH_3)_{n-1}Ge_nI_{3n+1}$ which adopts the structure Ruddlesden and Popper are discussed in detail in this study as we mentioned before. The number n is an integer that can have any value between one and infinity. As n grows, starting at n = 1, where only the cations $CH_3(CH_2)_3NH_3$ (BA) are present in the structure, the cations CH_3NH_3 (MA) partially replace BA. We have thicker layers of inorganic perovskite when there are more MA cations in the crystal structure. As a result, n denotes the number of layers in the perovskite framework. It will have one layer if n = 1, two if n = 2, and so on. X-ray diffraction (XRD) analysis ha used to investigate the changes that take place during the gradual expansion of the unit cell each time a perovskite layer is added, with additional peaks appearing in the diagram at equal intervals at low 2θ angles (below 10°).[36] The as synthesized compounds were studied in terms of optical absorption in order to determine the optical bandgaps in the series, so that the evolution of quantum confinement and nonlinearity across the series could be evaluated.

2. Experimental Section

Starting Materials

GeO_2 (99.999%) solid, HI (57% w/w), H_3PO_2(50% w/w), and n-$CH_3(CH_2)_3NH_2$ aqueous solutions were purchased from Sigma-Aldrich. By neutralizing equimolar volumes of 57 percent w/w aqueous hydriodic acid (HI) and 40 percent w/w aqueous methylamine (CH_3NH_2), methylammonium iodide, CH_3NH_3I (MAI) was produced.

Nomenclature note3D $CH_3NH_3GeI_3$ perovskite as $MAGeI_3$ and the 2D (n-$CH_3(CH_2)_3NH_3)_2(CH_3NH_3)_{n-1}Ge_nI_{3n+1}$ family as $(BA)_2(MA)_{n-1}Ge_nI_{3n+1}$ (n = 4, 3, 2, 1).

Syntheses

Two series of experiments were performed on the compositions of the Perovskites. *Method 1* was used to characterize the perovskites by powder x-ray diffraction and absorbance measurements. *Method 2* was used to determine the crystal structures via Single Crystal XRD.

Method 1

$MAGeI_3$ (n =∞). A vial was charged with GeO_2 (1mmol, 0.105gr) powder, aqueous solution of HI (57% w/w in H_2O, 5.1ml,38.7 mmol), and a magnetic stirring bar. The mixture was heated to boiling (~130°C), under continuous magnetic stirring. An orange powder (GeI_4) precipitated in the solution after about ten minutes. After its precipitation was complete, aqueous H_3PO_2 (50% w/w in H_2O, 1.7ml,15.5 mmol) was added at this point, and the solution turned to a clear bright yellow solution after roughly ten minutes. A dark red powder precipitated immediately when solid methylammonium iodide CH_3NH_3I (0.42mmol,0.067gr) was added to the solution, but it then quickly redissolved and the solution turned clear yellow again. Subsequently, 1.7ml of H_2O was added, the stirring was stopped, and the solution was left to cool to ambient temperature (~30 min) to produce dark red polyhedral crystals. The crystals were isolated via vacuum filtration. Yield: 80% based on total methylammonium used.

Method 2

$MAGeI_3$ (n =∞). The same procedure was followed with the corresponding iodide perovskite. The following quantities were used. GeO_2 (1mmol, 0.105gr) powder, aqueous solution of HI (5.1ml), H_3PO_2(1.7ml,15.5mmol), CH_3NH_3Cl (1mmol,0.067gr), 1.7ml H_2O .

Method 1

$(BA)_2(MA)_3Ge_4I_{13}$ (n = 4). A vial was filled with GeO_2(1mmol,0.105gr) powder, aqueous solution of HI (5.1ml, 38.7mmol), and a magnet. At 230°C, the mixture was subjected to continual thermal magnetic agitation. An orange powder precipitated in the solution after about six minutes. Aqueous H_3PO_2(1,7ml, 15.5mmol) was added at this point, and the solution turned a clear bright yellow after roughly seven minutes. The black powder precipitated when the solid methylammonium iodide CH_3NH_3I (0.28mmol,0.045gr) was added right away, but it quickly dissolved, and the solution

turned clear yellow again. In a separate beaker, n-$CH_3(CH_2)_3NH_2$ (100μL, 1 mmol) and H_2O (1.7ml) were added, thus yielding in a clear solution. Vapor formation was observed by pouring this content to the initial GeI_2 solution. The solution was then allowed to cool to room temperature overnight without stirring, resulting in the formation of red crystals like little thin rods. Suction filtration was used to isolate the crystals. Yield: 20% based on total methylammonium used.

Method 2

$(BA)_2(MA)_3Ge_4I_{13}$ (n = 4). The same procedure was followed with the corresponding iodide perovskite. The following quantities were used. GeO_2 (1mmol, 0.105gr) powder, aqueous solution of HI (5.1ml), H_3PO_2(1.7ml,15.5mmol), CH_3NH_3Cl (0.66mmol,0.045gr), n-$CH_3(CH_2)_3NH_2$ (100μL,1 mmol) ,1.7ml H_2O .

Method 1

$(BA)_2(MA)_2Ge_3I_{10}$ (n = 3). A vial was filled with GeO_2 (1mmol,0.105gr) powder, aqueous solution of HI (3.4ml, 25.8mmol), and a magnet. At 240°C, the mixture was subjected to continual thermal magnetic agitation. An orange powder precipitated in the solution after about five minutes. Aqueous H_3PO_2(1,7ml, 15.5mmol) was added at this point, and the solution turned a clear bright yellow after roughly nine minutes. The black powder precipitated when the solid methylammonium iodide CH_3NH_3I (0.28mmol,0.045gr) was added right away, but it quickly dissolved, and the solution turned clear yellow again. In a separate beaker, n-$CH_3(CH_2)_3NH_2$ (150μL, 1.5 mmol) and H_2O(1.7ml) were added, thus yielding in a clear solution. Vapor formation was observed by pouring this content to the initial GeI_2 solution. The solution was then allowed to cool to room temperature overnight without stirring, resulting in the formation of red crystals like little thin rods. Suction filtration was used to isolate the crystals. Yield: 20% based on total methylammonium used.

Method 2

$(BA)_2(MA)_2Ge_3I_{10}$ (n = 3). The same procedure was followed with the corresponding iodide perovskite. The following quantities were used. GeO_2 (1mmol, 0.105gr) powder, aqueous solution of HI (3.4ml), H_3PO_2(1.7ml,15.5mmol), CH_3NH_3Cl (0.66mmol,0.045gr), n-$CH_3(CH_2)_3NH_2$ (150μL,1.5 mmol) ,1.7ml H_2O .

Method 1

$(BA)_2(MA)Ge_2I_7$ (n = 2). A vial was filled with GeO_2 (1mmol,0.105gr) powder, aqueous solution of HI (3.4ml,25.8 mmol), and a magnet. At 240°C, the mixture was subjected to continual thermal magnetic agitation. An orange powder precipitated in the solution after about five minutes. Aqueous H_3PO_2(1,7ml, 15.5 mmol) was added at this point, and the solution turned a clear bright yellow after roughly six minutes. The black powder precipitated when the solid methylammonium iodide CH_3NH_3I (0.28mmol, 0.045gr) was added right away, but it quickly dissolved, and the solution turned clear yellow again. In a separate beaker, n-$CH_3(CH_2)_3NH_2$ (200 μL, 2 mmol) and H_2O(1.7ml) were added, thus yielding in a clear solution. Vapor formation was observed by pouring this content to the initial GeI_2 solution. The solution was then allowed to cool to room temperature overnight without stirring, resulting in the

formation of orange crystals in the shape of thin plates. Suction filtration was used to isolate the crystals. Yield: 20% based on total methylammonium used.

Method 2

$(BA)_2(MA)Ge_2Cl_7$ (n = 2). The same procedure was followed with the corresponding iodide perovskite. The following quantities were used. GeO_2 (1mmol, 0.105gr) powder, aqueous solution of HI (3.4ml), (1.7ml,15.5mmol), CH_3NH_3Cl (0.66mmol,0.045gr), n-$CH_3(CH_2)_3NH_2$ (200μL,2mmol) ,1.7ml H_2O .

Method 1

$(BA)_2GeI_4$ (n = 1). A vial was filled with GeO_2 (1mmol,0.105gr) powder, aqueous solution of HI (5,1ml, 38.7mmol), and a magnet. At 240°C, the mixture was subjected to continual thermal magnetic agitation. An orange powder precipitated in the solution after about five minutes. Aqueous H_3PO_2(1,7ml, 15.5mmol) was added at this point, and the solution turned a clear bright yellow after roughly five minutes. In a separate beaker, n-$CH_3(CH_2)_3NH_2$ (200 μL, 2 mmol) and H_2O(1.7ml) were added, thus yielding in a clear solution. Vapor formation was observed by pouring this content to the initial GeI_2 solution. The solution was then allowed to cool to room temperature overnight without stirring, resulting in the formation of orange crystals like little thin rods. Suction filtration was used to isolate the crystals. Yield: 20% based on total methylammonium used.

Method 2

$(BA)_2GeI_4$ (n = 1). The same procedure was followed with the corresponding iodide perovskite. The following quantities were used. GeO_2 (1mmol, 0.105gr) powder, aqueous solution of HI(5.1ml), H_3PO_2(1.7ml,15.5mmol), n-$CH_3(CH_2)_3NH_2$ (200μL,2mmol) ,1.7ml H_2O .

Characterization

Single-Crystal X-ray Diffraction

Full-sphere data were collected using a Bruker D8 VENTURE diffractometer equipped with a Kappa goniometer stage, a PHOTON II CPAD detector, and an IμS 3.0 Mo Kα source (λ = 0.71073 Å). Data were collected at 293 K. The collected data were integrated and applied with multiscan absorption correction using the APEX3 software. Crystal structures were solved by charge flipping and refined (full-matrix least-squares on F2) using the Jana2006 package

Powder X-ray Diffraction

A Bruker D8 Advance X-ray powder diffractometer (Cu Ka, 1.5406 Å) operating at 40 kV and 40 mA with a LynxEye Detector employing the Bragg-Brentano measuring geometry was used to make XRD powder measurements. The samples were mounted on glass in powder form and the data were obtained for angles 2θ =2 - 60°.

UV/vis Absorption Spectroscopy

A Shimadzu UV2600 Plus dual-beam spectrometer with an integration sphere in the 185-1400 nm range was used to acquire optical diffuse spectra. The powder is placed in a $BaSO_4$ sample container with a smooth surface that acts as a 100% reflection

reference. As seen in the optical characterization below, the reflectance spectra were converted to absorption spectra via the Kubelka-Munk transformation $\alpha/S = (1-R^2)/2R$.

Scanning Electron Microscope (SEM) measurements

SEM imaging and elemental microprobe analyses were performed using a JEOL JSM-6390LV SEM system equipped with an Oxford INCA PentaFETx3 EDS detector (Oxfordshire, UK). Data acquisition was performed using an accelerating voltage of 20 kV and a 60 s accumulation time.

3.Results and Discussion

3.1 Synthesis Description and chemical characterization of the samples

The synthesis of the 2D perovskites of the family $(CH_3(CH_2)_3NH_3)_2(CH_3NH_3)_{n-1}Ge_nI_{3n+1}$ with n = 1-4, as well as the 3D perovskite, was performed by precipitation of crystals from a solution of hydroiodic acid in the presence of a suitable reducing agent (H_3PO_2) to create and stabilize in the solution the (+2) oxidative state of germanium $Ge^{2+}$and to prevent the formation of the state Ge^{4+}.

We get GeI_4 (orange powder) when GeO_2 reacts with an aqueous solution of hydroiodic acid. The oxidative state of +4 of Germanium Ge^{4+} is maintained in the solid at this stage of the reaction. The oxidative state Ge^{2+} is formed when GeI_4 combines with the reducing agent H_3PO_2. As a result, the orange solid dissolves, and a clear yellow solution containing Ge^{2+}results. The small organic cation salt CH_3NH_3I is then added, and it dissolves almost instantly to produce a clear solution. When the resulting solution is allowed to cool to ambient temperature, 3D perovskite crystals (in the case of pure methylammonium addition) or 2D perovskite crystals (in the case of purr butylammonium addition or mixed methylammonium/butylammonium addition) will form. It was found that when a solution of butylamine in water (stoichiometric amount in 1.7mL of water) is added, the resulting solution that produces the 2D crystals is also resistant to oxidation in air.

It's important to note that hydroiodic acid at a 57% w/w concentration is an azeotropic mixture with a boiling point of 127° C. To get 127 ^{0}C on the hot plate where the reaction takes place, the temperature was set at 230 ^{0}C or 240 ^{0}C at the start of the reaction using only GeO_2 and aqueous HI. A word of caution here dictates that, because the H_3PO_2 solution is flammable when in direct contact with the hotplate, the temperature of the hotplate was decreased during the addition. During the reaction, a microscope slide was placed on the open end of the scintillation vial to maintain the liquid gas equilibrium (reflux conditions) and to maintain a homogeneous reaction temperature throughout the reaction flask.

For the analysis of the samples and to investigate if the reaction products are in agreement with the stoichiometry used, and check if there are impurities in the samples (mainly check if GeI_4 is present) since germanium oxidizes very easily in ambient air, X-ray diffraction (XRD) measurements were performed.

$(BA)_2GeI_4$ (n = 1)

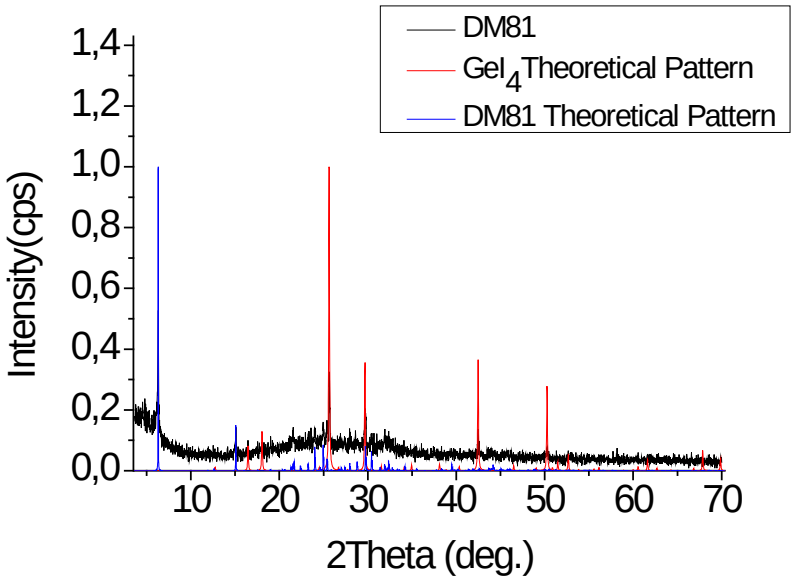

Figure 4. XRD diagram of the compound BA_2GeI_4

From the analysis of the diagrams for BA_2GeI_4 (**Figure 4**), oxidation of the material was observed, mainly in the form of GeI_4 as indicated by the red peaks from the simulated pattern which appear at the 2θ angles of 25.7^0, 29.7^0, 42.5^0 and 50.5^0. Also, a peak appears at the angle $2\theta = 6.3^0$ corresponding to the blue peak of the theoretical pattern for n = 1. This angle 6.3^0 is characteristic for a sample pattern n = 1. It's likely that this oxidation occurs because the time interval between sample preparation and the actual measurement is more than 12 hours, which is a typical stability of the Ge compounds in air. Another reason may arise from the XRD sample preparation method. The surface of the solution which is in direct contact with air, tend to oxidize over time and to form a "crust" of GeI_4 crystals near the surface. Fortunately, this crust is impermeable to oxygen and thus the solution is protected from further oxidation in the vial. Nevertheless, the presence of the crust itself makes it difficult to separate the crystals of the Ge^{2+} product from the bottom of the vial without disturbing the oxidized crust.

The flattened peak of the sample, which extends throughout a large range of Bragg angles (2θ), roughly 20^0 to 40^0, as seen in the experimental pattern is caused by an amorphous material, which can be either the soda lime crust substrate or grease used to hold the powder sample in place.

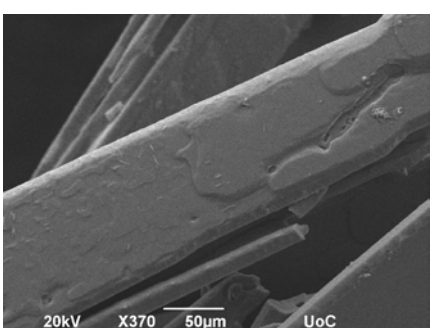

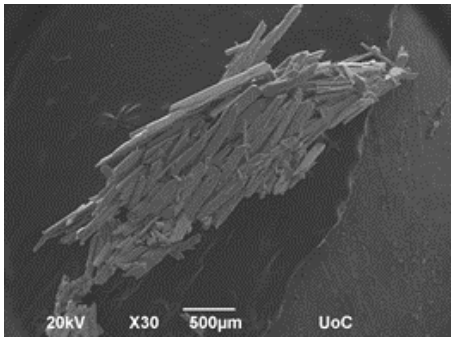

Element	App Conc.	Intensity Corrn.	Weight%	Weight% Sigma	Atomic%
C K	14.49	0.8091	17.86	1.21	68.95
N K	-0.13	0.2558	-0.50	1.84	-1.66
Ge L	3.19	0.3455	9.21	0.87	5.88
I L	68.06	0.9246	73.43	1.85	26.82
Totals			100.00		

Figure 5. SEM images (top) and EDS analysis (bottom) for selected crystals of the compound BA_2GeI_4

The surface of the crystalline BA_2GeI_4 compound was characterized via Scanning Electron Microscopy (SEM) measurements, and Electron Dispersive X-ray Spectroscopy (EDS) for elemental analysis (Figure 5). Typical crystals BA_2GeI_4 have a rod-like shape and show no sign of degradation for the majority of the crystals. The elemental analysis reveals Ge:I ratio of 1:4.6, in good agreement with the expected stoichiometry.

$(BA)_2(MA)Ge_2I_7$ (n = 2)

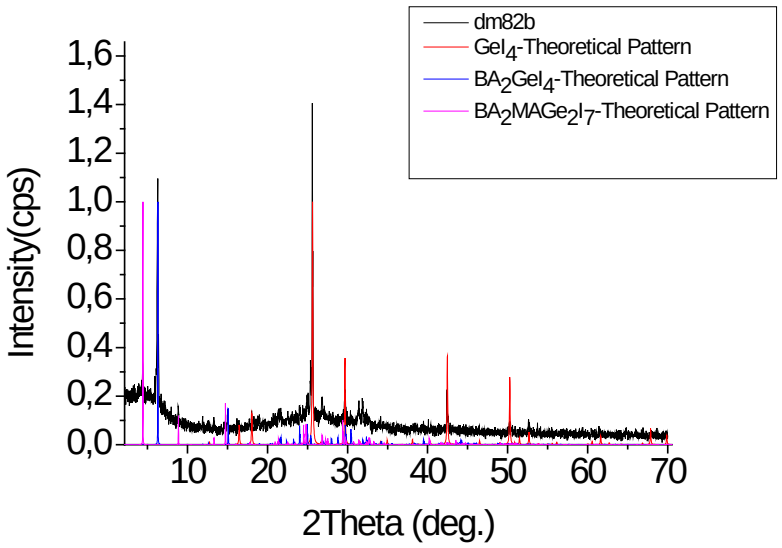

Figure 6. XRD diagram of the powder obtained from the nominal synthesis of the compound $BA_2(MA)Ge_2I_7$ (n = 2)

A similar situation arises in the case of the reaction designed to perform the synthesis of $BA_2(MA)Ge_2I_7$ (n = 2) (**Figure 6**). The oxidation of the $BA_2(MA)Ge_2I_7$ can be seen in the red peaks corresponding to the simulated pattern of GeI_4, that appear at angles of 25.6^0, 29.7^0, 42.5^0, and 50.2^0 on the XRD pattern. At 6.3^0, a peak appears once more, which corresponds to the theoretical peak of the blue pattern for n = 1, which is the major product of the reaction. As a result, it is determined that the desired perovskite $(BA)_2(MA)Ge_2I_7$ (n = 2) has not been synthesized successfully, but only as a minor product of the reaction. According to the simulated pattern for $(BA)_2(MA)Ge_2I_7$, peaks at 4.4^0 and 9.3^0 would be required for a perovskite to form at n = 2, which only appear as a weak signal.

$(BA)_2(MA)_2Ge_3I_{10}$ (n = 3)

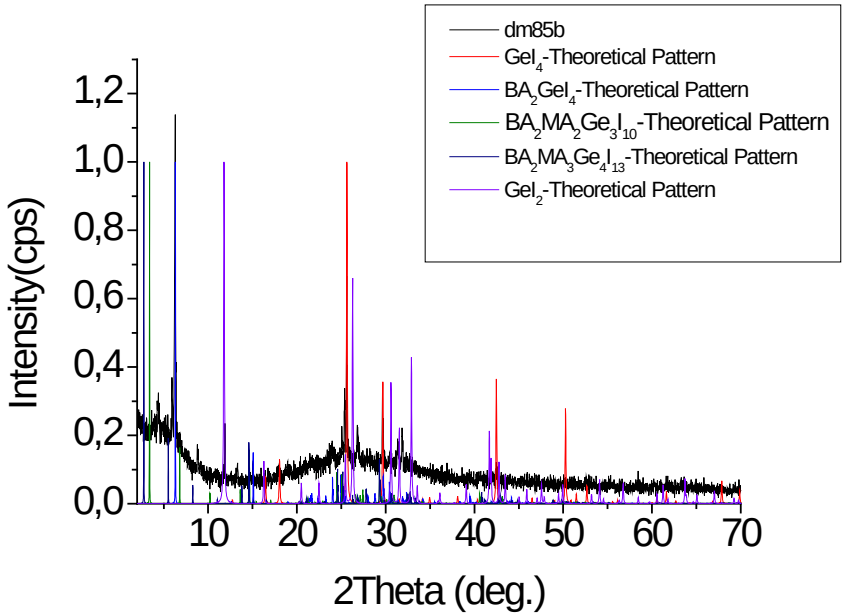

Figure 7. XRD diagram of the powder obtained from the nominal synthesis of the compound $BA_2(MA)_2Ge_3I_{10}$ (n = 3)

A similar situation arises in the case of the reaction designed to perform the synthesis of $BA_2(MA)_2Ge_3I_{10}$ (n = 3) (**Figure 7**). The appearance of peaks at angles 25.6^0 and 29.7^0 in the XRD pattern indicates that the material is indeed oxidized. There is a peak at angle 6.3^0, which corresponds to the theoretical pattern of n = 1, and at angle 14.6^0, which corresponds to the theoretical pattern of n = 4, respectively. There is also a small amount of GeI_2 at an angle of 11.8^0. As a result, instead of the expected perovskite $(BA)_2(MA)_2Ge_3I_{10}$, a mixture with n = 1 and n = 4 as well as quantities of GeI_4 and GeI_2 was formed. According to the theoretical pattern for n = 3, peaks should appear at angles 3.4^0, 6.8^0 and 10.2^0. Again, there is a flattened top from 20^0-40^0. The noise in the black pattern for angles below 10^0 is due to the holder, which is made of polymer material, on which the glass with the sample is placed.

$(BA)_2(MA)_3Ge_4I_{13}$ (n = 4)

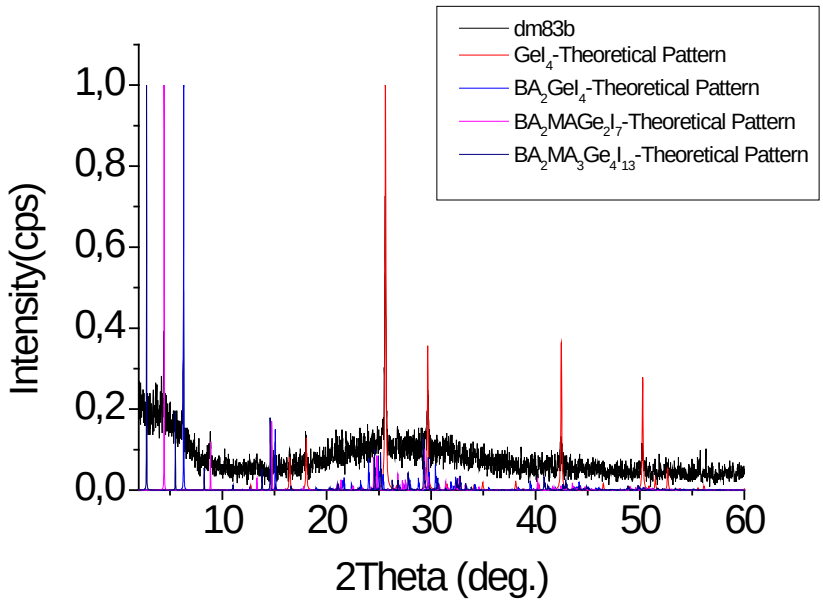

Figure 8. XRD diagram of the powder obtained from the nominal synthesis of the compound $BA_2(MA)_3Ge_4I_{13}$ (n = 4)

Likewise, for $BA_2(MA)_3Ge_4I_{13}$ (n = 4) (**Figure 8**) the oxidized product is the dominant feature of the XRD pattern. At angle 6.3^0, which corresponds to the theoretical pattern for n = 1, and at angle 4.4^0, which corresponds to the theoretical pattern for n = 2, there is a peak. As a result, the anticipated perovskite, $(BA)_2(MA)_3Ge_4I_{13}$ for n = 4, was not synthesized, but rather a mixture of n = 1 and n = 2 was obtained. Peaks should arise at angles 2.7^0, 5.4^0, 8.3^0, and 11.1^0, according to the theoretical range for n = 4. Due to the amorphous glass, a flattened top is noticed in the region of 20^0-40^0 angles. There is also noise at angles below 10^0 owing to the polymer holder.

4.2 Description of the Crystal Structures

2D perovskite crystal structure with n = 1

The orthorhombic structure of the perovskite $(BA)_2GeI_4$ (n = 1) is depicted in **Figure 9** while selected crystallographic parameters are listed in Tables 1-4. The compound crystallizes in the noncentrosymmetric space group $Pna2_1$ with four formula units in the unit cell. Individual GeI_4^{2-} sheets are created by $[GeI_6]4-\text{corner}-$ sharin octahedra, with double layers of butylammonium cations arranged along the a-crystallographic axis, separate the inorganic sheets from one another. The cation's$-NH_3^+$ "polar head" approaches the iodide on the octahedron's vertical axis a and points to the center of the rhombic cavity formed by four adjacent octahedrons. The electrostatic attraction between the positively charged head and the negatively charged inorganic lattice is the driving force behind this interaction.

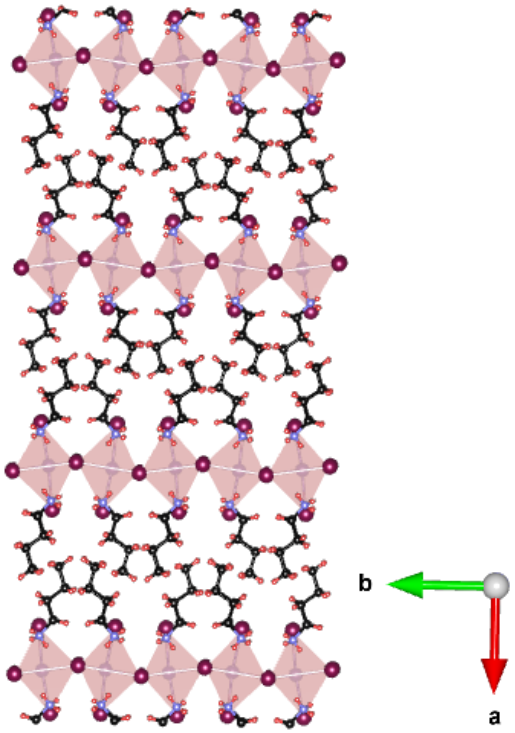

Figure 9. Crystal structure of the 2D germanium iodide perovskite, $(BA)_2GeI_4$ (n=1). The atoms are color-coded as follows: ● I, ●Ge, ● N, ● C, ● H.

The "tail"$-CH_3$ denotes the interstitial area between the layers of inorganic perovskite, where nonpolar dispersion forces dominate the secondary interactions of the organic component of the structure. Because the integration of the BA spacers, which is a relatively long organic chain comprising of four carbon atoms, requires some vacant space to fit, the separation of the inorganic layers causes a rise in the lattice constants. The octahedra appear to tilt alternatively along the b-axis, causing the sheets to groove. The I-Ge-I bond angle deviates significantly from 90 degrees (Table 3), clearly indicating the grooving of the lattice. The distortion of germanium-iodine octahedrons is caused by the fact that germanium contains a lone pair of electrons in its valence shell that isn't engaged in chemical bonding. As a result, it takes up space where it is inserted, causing elongation at the Ge-I bonds in the direction the lone pair is expressed. Two short and four long bonds are generated, as shown in the Table 1.

Table 1. Bond length [Å] for $(BA)_2GeI_4$ at 293 K with estimated standard deviations in parentheses.

Label	Distance
I(1)-Ge(1)	2.777(2)
I(2)-Ge(1)'	3.0603(9)
I(3)-Ge(1)	3.0204(9)
I(4)-Ge(1)	2.802(2)

Table 2. Crystal data and structure refinement for $(BA)_2GeI_4$ at 293 K.

Empirical formula	$(BA)_2GeI_4$
Formula weight	728.5
Temperature	293 K
Wavelength	0.71073 Å
Crystal system	orthorhombic
Space group	P n a 21
Unit cell dimensions	a = 28.0299(6) Å, α = 90° b = 8.7239(5) Å, β = 90° c = 8.281(2) Å, γ = 90°
Volume	2024.8(5) $Å^3$
Z	4
Density (calculated)	2.3897 g/cm^3
Absorption coefficient	7.595 mm^{-1}
F(000)	1320
θ range for data collection	2.45 to 30.1°
Index ranges	-39<=h<=39, -12<=k<=12, -11<=l<=10
Reflections collected	93281
Independent reflections	3610 [R_{int} = 0.0428]
Completeness to θ = 30.1°	99.00%
Refinement method	Full-matrix least-squares on F^2
Data / restraints / parameters	3610 / 14 / 79
Goodness-of-fit	2.74
Final R indices [I>2σ(I)]	R_{obs} = 0.0424, wR_{obs} = 0.1078
R indices [all data]	R_{all} = 0.0503, wR_{all} = 0.1094
Largest diff. peak and hole	0.83 and -1.00 $e \cdot Å^{-3}$

Table 3. Bond angle [°] for $(BA)_2GeI_4$ at 293 K with estimated standard deviations in parentheses.

Label	Angle
I(2)'0-Ge(1)-I(3)	173.85(3)

Table 4. Atomic coordinates ($x10^4$) and equivalent isotropic displacement parameters ($Å^2x10^3$) for $(BA)_2GeI_4$ at 293 K with estimated standard deviations in parentheses.

Label	x	y	z	Occupancy	Ueq*
I(1)	0.2383(1)	0.2267(2)	0.2504(2)	1	0.076(1)
I(2)	0.1438(1)	0.5443(1)	-0.0029(2)	1	0.085(1)
I(3)	0.1418(1)	-0.0557(1)	0.4976(2)	1	0.081(1)
I(4)	0.2379(1)	0.2297(2)	0.7435(2)	1	0.074(1)
Ge(1)	0.2475(1)	0.0124(1)	0.4963(3)	1	0.062(1)
N(1)	0.6637(3)	0.5543(12)	-0.0300(20)	1	0.161(3)
N(2)	0.1662(3)	0.5376(13)	0.4660(20)	1	0.150(3)
C(1)	0.6263(3)	0.4478(13)	0.0277(18)	1	0.161(3)
C(2)	0.5790(3)	0.4885(9)	-0.0510(20)	1	0.161(3)
C(3)	0.5483(3)	0.3454(10)	-0.0646(18)	1	0.161(3)
C(4)	0.4961(3)	0.3910(17)	-0.0710(20)	1	0.161(3)
C(5)	0.1281(3)	0.4334(12)	0.5231(18)	1	0.150(3)
C(6)	0.0805(3)	0.4832(9)	0.4530(20)	1	0.150(3)
C(7)	0.0485(3)	0.3441(10)	0.4320(17)	1	0.150(3)

*U_{eq} is defined as one third of the trace of the orthogonalized U_{ij} tensor.

2D perovskite crystal structure with n = 2

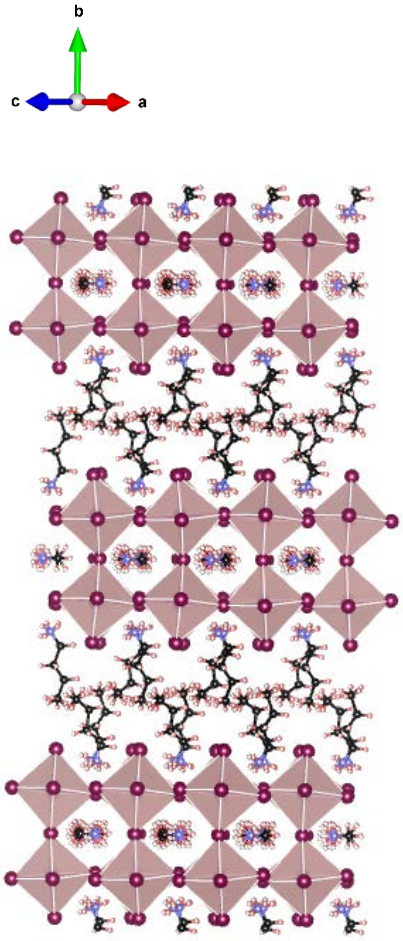

Figure 10 : Crystal structure of the 2D germanium iodide perovskite, (BA)2(MA)n−1GenI3n+1 with n=2. The following is the symbolism of the atoms: ● I, ●Ge, ● N, ● C, ● H.

The orthorhombic structure of the perovskite $(BA)_2(MA)Ge_2I_7$ (n= 2) is depicted in **Figure 10** while selected crystallographic parameters are listed in Tables 5-8. The compound crystallizes in the noncentrosymmetric space group *Amm*2 with four formula units in the unit cell. Compared to n = 1 the are some important differences. The inorganic perovskite layers are also made up of layers of GeI_6 corner − sharing octahedra. This time, however, they are made up of two layers of germanium-iodine octahedra that are connected by individual Ge-I-Ge bridges along the crystallographic b-axis. Rhombic cavities are generated in this arrangement, as indicated in the figure. The cations of $CH_3NH_3^+$ methylammonium, which are oriented along the crystallographic ac plane, are held within these cavities. The head $-NH_3^+$ approaches the iodides forming weak hydrogen bonds $NH_2 - H \cdots I - Ge$, just as it does with the BA cations, and these bond points to the center of the rhombic cavity formed by four surrounding octahedrons. The $-NH_3^+$ head of MA is oriented in the direction of the a-axis for the first two rhombic cavities in the first double inorganic layer, and afterwards to the c-axis. All the heads in the second double inorganic layer point to the c axis. The same order is followed in the third inorganic layer as it was in the first.

The layers are also separated from one another along the b-axis by bilayers of BA cations, which heads $-NH_3^+$ and tails $-CH_3$ generate the same interactions as in structure n = 1. In addition, the BA cations deform the perovskite along the b-axis, whereas the MA cations distort it about the ac- plane. As a result of the competition between the two cations, the intermediate 2D perovskites undergo total deformation in two different directions, which is weaker than n = 1 due to the competition between MA and BA interactions. The stereoactivity of the lone electron pair also affects the length of the Ge-I bonds in this case, as seen in table 5.

Table 5. Bond lengths [Å] for $(BA)_2(MA)Ge_2I_7$ at 293 K with estimated standard deviations in parentheses.

Label	Distances
I(1)-Ge(2)’	3.171(6)
I(2)-Ge(1)’	2.838(3)
I(3)-Ge(1)	3.237(4)
I(3)-Ge(2)’	2.862(3)
I(4)-Ge(1)	2.937(6)

I(5)-Ge(1)’	3.195(5)

Table 6. Crystal data and structure refinement for $(BA)_2(MA)Ge_2I_7$ at 293 K.

Empirical formula	$(BA)_2(MA)Ge_2I_7$
Formula weight	1213.9
Temperature	293 K
Wavelength	0.71073 Å
Crystal system	orthorhombic
Space group	A m m 2
Unit cell dimensions	a = 8.5148(13) Å, α = 90° b = 39.866(7) Å, β = 90° c = 8.6668(13) Å, γ = 90°
Volume	2941.9(8) $Å^3$
Z	4
Density (calculated)	2.7406 g/cm^3
Absorption coefficient	9.389 mm^{-1}
F(000)	2160
Crystal size	? x ? x ? mm^3
θ range for data collection	2.39 to 26.49°
Index ranges	-10<=h<=10, -49<=k<=49, -10<=l<=10
Reflections collected	31650
Independent reflections	2905 [R_{int} = 0.1363]
Completeness to θ = 26.49°	100%
Refinement method	Full-matrix least-squares on F^2
Data / restraints / parameters	2905 / 16 / 80
Goodness-of-fit	1.65
Final R indices [I>2σ(I)]	R_{obs} = 0.0762, wR_{obs} = 0.1266
R indices [all data]	R_{all} = 0.1302, wR_{all} = 0.1371
Extinction coefficient	?
Largest diff. peak and hole	1.92 and -1.80 e·$Å^{-3}$

$R = \Sigma||F_o|-|F_c|| / \Sigma|F_o|$, $wR = \{\Sigma[w(|F_o|^2 - |F_c|^2)^2] / \Sigma[w(|F_o|^4)]\}^{1/2}$ and $w=1/(\sigma^2(I)+0.0004I^2)$

Table 7. Bond angles [°] for $(BA)_2(MA)Ge_2I_7$ at 293 K with estimated standard deviations in parentheses.

Label	Angles
Ge(2)-I(1)-Ge(2)’	164.94(15)
Ge(1)-I(5)-Ge(1)’	179.47(13)

Table 8. Atomic coordinates ($x10^4$) and equivalent isotropic displacement parameters ($Å^2x10^3$) for $(BA)_2(MA)Ge_2I_7$ at 293 K with estimated standard deviations in parentheses.

Label	x	y	z	Occupancy	U_{eq}*
I(1)	0.5000	0.0000	-0.2199(4)	1	0.078(2)
I(2)	0.2443(3)	0.4173(1)	0.0487(3)	1	0.084(1)
I(3)	0.2538(3)	0.0720(1)	0.0508(3)	1	0.086(1)
I(4)	0.0000	0.1530(1)	0.2741(3)	1	0.108(2)
I(5)	0.0000	0.5000	-0.1720(3)	1	0.093(2)
I(6)	0.5000	0.3480(1)	0.3569(4)	1	0.104(2)
Ge(1)	0.0000	0.0802(2)	0.3263(4)	1	0.071(2)
Ge(2)	0.5000	0.4211(2)	0.3281(4)	1	0.076(2)
N(1)	0.5000	0.0000	0.3040(80)	1	0.340(40)
N(2)	0.0000	0.5000	-0.5580(80)	1	0.280(30)
N(3)	0.0000	0.3667(6)	0.3530(40)	1	0.203(10)
N(4)	0.5000	0.3671(13)	-0.2120(70)	1	0.383(19)
C(1)	0.5000	0.0000	0.4750(80)	1	0.340(40)
C(2)	0.0000	0.5000	-0.7290(80)	1	0.280(30)
C(3)	0.0000	0.3403(6)	0.2330(30)	1	0.203(10)
C(4)	0.0000	0.3060(6)	0.3090(20)	1	0.203(10)
C(5)	0.0000	0.2789(7)	0.1860(30)	1	0.203(10)
C(6)	0.0000	0.2446(6)	0.2630(50)	1	0.203(10)
C(7)	0.5000	0.3305(13)	-0.2400(50)	1	0.383(19)
C(8)	0.5000	0.3121(11)	-0.0860(50)	1	0.383(19)
C(9)	0.5000	0.2745(11)	-0.1140(60)	1	0.383(19)
C(10)	0.5000	0.2562(13)	0.0400(80)	1	0.383(19)

*U_{eq} is defined as one third of the trace of the orthogonalized U_{ij} tensor.

2D perovskite crystal structure with n = 3

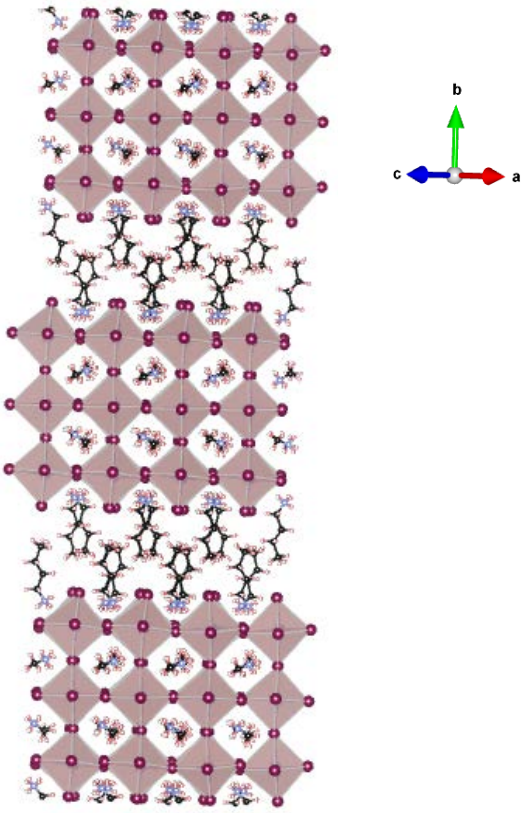

Figure11 Crystal structure of the 2D germanium iodide perovskite, (BA)2(MA)n−1GenI3n+1 with n=3 . The following is the symbolism of the atoms: ● I, ●Ge, ● N, ● C, ● H.

The orthorhombic structure of the perovskite $(BA)_2(MA)_2Ge_3I_{10}$ (n = 3) is depicted in **Figure 11** while selected crystallographic parameters are listed in Tables 9-12. The compound crystallizes in the noncentrosymmetric space group *Cmc*2_1 with four formula units in the unit cell. $(BA)_2(MA)_2Ge_3I_{10}$ (n = 3) has an orthorombic structure that is similar to n = 2. The number of layers that make up the inorganic perovskite lattice differs. Three layers of octahedrons are connected along the b-axis by their corners. The MA cations are deposited in the rhombic cavities once more, but this time they are not aligned along the a and c axis. They've adopted a diagonal slope. However, they interact with octahedrons in the same way. The BA cations separate the layers along the b-axis, having the same effect on the structure as the previous ones. In the deformation of the MA and BA cations in two opposite orientations, there is once again competition.

Table 9. Bond lengths [Å] for $(BA)_2(MA)_2Ge_3I_{10}$ at 293 K with estimated standard deviations in parentheses.

Label	Distances
I(1)-Ge(3)	3.023(3)
I(2)-Ge(3)	2.7626(18)
I(3)-Ge(1)	2.7702(15)
I(5)-Ge(1)	3.168(2)
I(5)-Ge(3)	3.085(3)
I(6)-Ge(1)	2.937(2)

Table 10. Crystal data and structure refinement for $(BA)_2(MA)_2Ge_3I_{10}$ at 293 K.

Empirical formula	$(BA)_2(MA)_2Ge_3I_{10}$
Formula weight	1699.2
Temperature	293 K
Wavelength	0.71073 Å
Crystal system	orthorhombic
Space group	C m c 21
Unit cell dimensions	a = 8.4756(9) Å, α = 90° b = 51.989(5) Å, β = 90° c = 8.7551(8) Å, γ = 90°
Volume	3857.9(7) $Å^3$
Z	4
Density (calculated)	2.9256 g/cm^3
Absorption coefficient	10.333 mm^{-1}
F(000)	3000
Crystal size	? x ? x ? mm^3
θ range for data collection	2.35 to 30.77°
Index ranges	-12<=h<=12, -74<=k<=74, -12<=l<=12
Reflections collected	94899
Independent reflections	3754 [R_{int} = 0.0869]
Completeness to θ = 30.77°	9800%
Refinement method	Full-matrix least-squares on F^2
Data / restraints / parameters	3754 / 16 / 103
Goodness-of-fit	2.58
Final R indices [I>2σ(I)]	R_{obs} = 0.0564, wR_{obs} = 0.1256
R indices [all data]	R_{all} = 0.0628, wR_{all} = 0.1274
Extinction coefficient	?
Largest diff. peak and hole	1.70 and -1.12 e·$Å^{-3}$

$R = \Sigma||F_o|-|F_c|| / \Sigma|F_o|$, $wR = \{\Sigma[w(|F_o|^2 - |F_c|^2)^2] / \Sigma[w(|F_o|^4)]\}^{1/2}$ and $w=1/(\sigma^2(I)+0.0004I^2)$

Table 11. Bond angles [°] for $(BA)_2(MA)_2Ge_3I_{10}$ at 293 K with estimated standard deviations in parentheses.

Label	Angles
Ge(1)-I(5)-Ge(3)	164.51(6)

Table 12. Atomic coordinates ($x10^4$) and equivalent isotropic displacement parameters ($Å^2x10^3$) for $(BA)_2(MA)_2Ge_3I_{10}$ at 293 K with estimated standard deviations in parentheses.

Label	x	y	z	Occupancy	U_{eq}^*
I(1)	0.0000	0.3082(1)	0.2317(2)	1	0.065(1)
I(2)	0.2435(2)	0.2483(1)	0.0102(2)	1	0.079(1)
I(3)	0.2426(2)	0.1362(1)	0.0003(2)	1	0.066(1)
I(4)	0.2428(2)	0.3719(1)	0.0017(2)	1	0.067(1)
I(5)	0.0000	0.1912(1)	0.2630(2)	1	0.064(1)
I(6)	0.0000	0.0746(1)	0.1854(2)	1	0.090(1)
I(7)	0.0000	0.4255(1)	0.2707(2)	1	0.081(1)
Ge(1)	0.0000	0.1309(1)	0.2099(2)	1	0.050(1)
Ge(2)	0.0000	0.3712(1)	0.2127(2)	1	0.049(1)
Ge(3)	0.0000	0.2501(1)	0.2197(2)	1	0.052(1)
N(1)	0.0000	0.3095(1)	0.6541(2)	1	0.266(15)
N(2)	0.0000	0.1984(1)	0.8022(2)	1	0.350(20)
N(3)	0.5000	0.0901(1)	0.1890(2)	1	0.231(9)
N(4)	0.0000	0.0903(1)	0.7860(2)	1	0.267(10)
C(1)	0.0000	0.3021(1)	0.8174(2)	1	0.266(15)
C(2)	0.0000	0.1867(1)	0.6481(2)	1	0.350(20)
C(3)	0.5000	0.0694(1)	0.3048(2)	1	0.231(9)
C(4)	0.5000	0.0434(1)	0.2251(2)	1	0.231(9)
C(5)	0.5000	0.0221(1)	0.3439(2)	1	0.231(9)
C(6)	0.5000	-0.0039(1)	0.2642(2)	1	0.231(9)
C(7)	0.0000	0.0731(1)	0.6511(2)	1	0.267(10)
C(8)	0.0000	0.0452(1)	0.7034(2)	1	0.267(10)
C(9)	0.0000	0.0276(1)	0.5648(2)	1	0.267(10)
C(10)	0.0000	-0.0002(1)	0.6171(2)	1	0.267(10)

*U_{eq} is defined as one third of the trace of the orthogonalized U_{ij} tensor.

2D perovskite crystal structure with n = 4

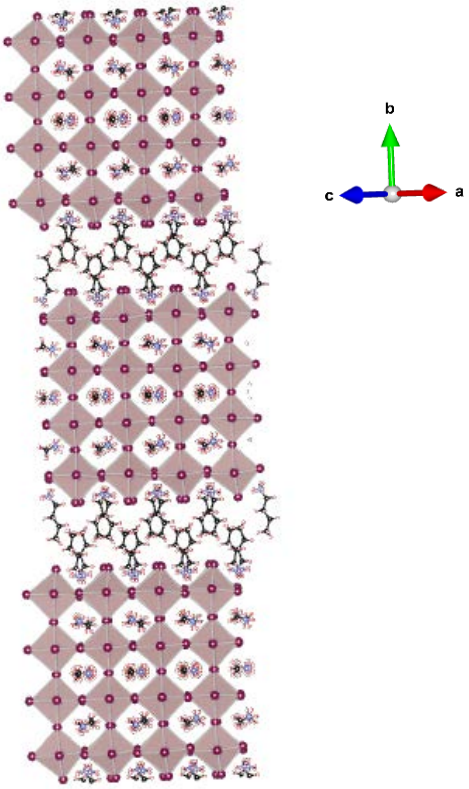

Picture9 : Crystal structure of the 2D germanium iodide perovskite, (BA)2(MA)n−1GenI3n+1 with n=4. The following is the symbolism of the atoms: ● I, ●Ge, ● N, ● C, ● H.

The orthorhombic structure of the perovskite $(BA)_2(MA)_3Ge_4I_{13}$ (n = 4) is depicted in **Figure 12** while selected crystallographic parameters are listed in Tables 13-16. The compound crystallizes in the noncentrosymmetric space group *Amm*2 with four formula units in the unit cell and it is similar to the structure for n = 2. The inorganic perovskite framework in this example is made up of four layers of corner – shared octahedra along b-axis. The MA cations are found in the rhombic cavities. In the first row of cavities in the inorganic lattice, the cation has a diagonal slope once more. With its axes c and a, it is not linear. It is aligned with the ac plane in the second row, and it has the same orientation as the first row in the third. The group $-NH_3^+$ interacts with the iodide of the octahedron via hydrogen bonds once again. The same interaction behavior of the BA cations separates the inorganic layers along the b-axis.

Table 13. Bond lengths [Å] for $(BA)_2(MA)_3Ge_4I_{13}$ at 293 K with estimated standard deviations in parentheses.

Label	Distances
I(6)-Ge(3)	3.2176(15)
I(8)-Ge(4)	2.7548(10)

Table 14. Crystal data and structure refinement for $(BA)_2(MA)_3Ge_4I_{13}$ at 293 K.

Empirical formula	$(BA)_2(MA)_3Ge_4I_{13}$
Formula weight	2184.6
Temperature	293 K
Wavelength	0.71073 Å
Crystal system	orthorhombic
Space group	A m m 2
Unit cell dimensions	a = 8.4767(3) Å, α = 90° b = 64.140(3) Å, β = 90° c = 8.7655(3) Å, γ = 90°
Volume	4765.8(3) $Å^3$
Z	4
Density (calculated)	3.0447 g/cm^3
Absorption coefficient	10.933 mm^{-1}
F(000)	3840
Crystal size	? x ? x ? mm^3
θ range for data collection	2.35 to 30.54°
Index ranges	-12<=h<=12, -91<=k<=91, -12<=l<=12
Reflections collected	146868
Independent reflections	4670 [R_{int} = 0.0505]
Completeness to θ = 30.54°	100%
Refinement method	Full-matrix least-squares on F^2
Data / restraints / parameters	4670 / 18 / 133
Goodness-of-fit	3.25
Final R indices [I>2σ(I)]	R_{obs} = 0.0436, wR_{obs} = 0.1127
R indices [all data]	R_{all} = 0.0454, wR_{all} = 0.1131
Extinction coefficient	?
Largest diff. peak and hole	1.83 and -1.14 e·$Å^{-3}$

$R = \Sigma||F_o|-|F_c|| / \Sigma|F_o|$, $wR = \{\Sigma[w(|F_o|^2 - |F_c|^2)^2] / \Sigma[w(|F_o|^4)]\}^{1/2}$ and $w=1/(\sigma^2(I)+0.0004I^2)$

Table 15. Bond angles [°] for $(BA)_2(MA)_3Ge_4I_{13}$ at 293 K with estimated standard deviations in parentheses.

Label	Angles
Ge(1)-I(3)-Ge(1)’	172.65(4)
Ge(4)-I(5)-Ge(4)’	166.22(4)
Ge(1)-I(6)-Ge(3)	164.78(4)

Table 16. Atomic coordinates ($x10^4$) and equivalent isotropic displacement parameters ($Å^2x10^3$) for $(BA)_2(MA)_3Ge_4I_{13}$ at 293 K with estimated standard deviations in parentheses.

Label	x	y	z	Occupancy	U_{eq}*
I(1)	0.5000	0.4051(1)	0.4203(1)	1	0.066(1)
I(2)	0.2425(1)	0.1398(1)	0.1867(1)	1	0.065(1)
I(3)	0.0000	0.0000	0.4321(1)	1	0.064(1)
I(4)	0.0000	0.1897(1)	0.3725(1)	1	0.089(1)
I(5)	0.5000	0.5000	0.4506(1)	1	0.064(1)
I(6)	0.0000	0.0949(1)	0.4498(1)	1	0.067(1)
I(7)	0.2572(1)	0.3537(1)	0.1880(1)	1	0.067(1)
I(8)	0.2564(1)	0.4536(1)	0.2005(1)	1	0.072(1)
I(9)	0.2431(1)	0.4878(1)	0.2007(1)	1	0.073(1)
I(10)	0.5000	0.3101(1)	0.4585(1)	1	0.081(1)
Ge(1)	0.0000	0.4841(1)	0.4094(2)	1	0.050(1)
Ge(2)	0.5000	0.3542(1)	0.3996(2)	1	0.048(1)
Ge(3)	0.0000	0.1445(1)	0.3959(2)	1	0.051(1)
Ge(4)	0.5000	0.4519(1)	0.4081(2)	1	0.048(1)
N(1)	0.0000	0.0000	-0.1796(1)	1	0.322(18)
N(2)	0.5000	0.5000	0.8310(1)	1	0.337(19)
N(3)	0.5000	0.0951(1)	0.4592(1)	1	0.287(11)
N(4)	0.0000	0.0882(1)	-0.1915(1)	1	0.550(20)
N(5)	0.0000	0.3221(1)	0.4548(1)	1	0.216(6)
N(6)	0.5000	0.1779(1)	0.3528(1)	1	0.290(8)
C(1)	0.0000	0.0000	-0.0107(1)	1	0.322(18)
C(2)	0.5000	0.5000	0.9999(1)	1	0.337(19)
C(3)	0.5000	0.0881(1)	0.2983(1)	1	0.287(11)
C(4)	0.0000	0.0932(1)	-0.0267(1)	1	0.199(11)
C(5)	0.0000	0.3059(1)	0.3341(1)	1	0.216(6)
C(6)	0.0000	0.2844(1)	0.4072(1)	1	0.216(6)
C(7)	0.0000	0.2678(1)	0.2833(1)	1	0.216(6)
C(8)	0.0000	0.2464(1)	0.3564(1)	1	0.216(6)
C(9)	0.5000	0.1912(1)	0.4909(1)	1	0.290(8)
C(10)	0.5000	0.2140(1)	0.4441(1)	1	0.290(8)
C(11)	0.5000	0.2277(1)	0.5859(1)	1	0.290(8)
C(12)	0.5000	0.2505(1)	0.5391(1)	1	0.290(8)

*U_{eq} is defined as one third of the trace of the orthogonalized U_{ij} tensor.

2D perovskite crystal structure with n = ∞

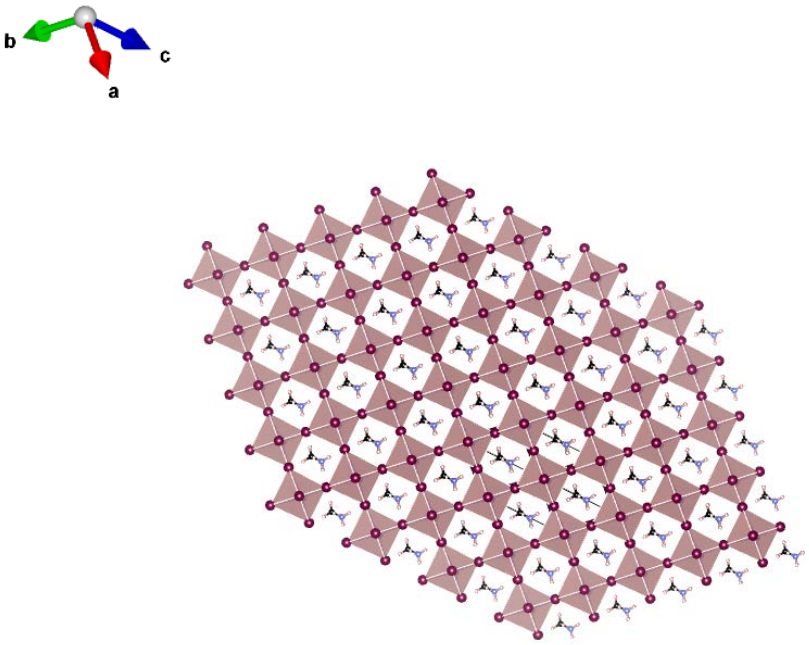

Figure 13: Crystal structure of the 2D germanium iodide perovskite, (BA)2(MA)n−1GenI_{3n+1} with n=∞. The following is the symbolism of the atoms: ● I, ●Ge, ● N, ● C, ● H.

The rhombohedral structure of the perovskite $MAGeI_3$ (n= ∞) is depicted in **Figure 13** while selected crystallographic parameters are listed in Tables 17-20. The compound crystallizes in the noncentrosymmetric space group *R*3*m* with four formula units in the unit cell. Its structure consists of trigonal pyramidal units $[GeI_3]^-$ around which organic MA cations are assembled. Single Ge-I-Ge bridges connect the octahedra to form $[GeI_6]^{4-}$angular octahedra. The octahedra take on a trigonal distorted structure, like $BaTiO_3$. In comparison to the original cubic construction, the volume of the unit cell is tripled due to the centering of the lattice. The deformation of the octahedra is again due to the stereoactivity of the single electron pair of the outer layer of germanium. The MA cation also plays a role in the deformation which is oriented along the rhombohedral crystallographic axis c. In the 3D structure there are no BA cations, because there is no space for them to fit. There are no layers to separate them.

Table 17. Bond lengths [Å] for $MAGeI_3$ at 293 K with estimated standard deviations in parentheses.

Label	Distances
I-Ge	2.7446(11)

Table 18. Crystal data and structure refinement for $MAGeI_3$ at 293 K.

Empirical formula	$MAGeI_3$
Formula weight	485.4
Temperature	293 K
Wavelength	0.71073 Å
Crystal system	trigonal
Space group	R 3 m
Unit cell dimensions	a = 8.4654(8) Å, α = 90° b = 8.4654(8) Å, β = 90° c = 11.0295(8) Å, γ = 120°
Volume	684.51(10) $Å^3$
Z	3
Density (calculated)	3.5323 g/cm^3
Absorption coefficient	13.413 mm^{-1}
F(000)	630
Crystal size	? x ? x ? mm^3
θ range for data collection	4.63 to 30.74°
Index ranges	-12<=h<=12, -12<=k<=12, -15<=l<=15
Reflections collected	6593
Independent reflections	328 [R_{int} = 0.0244]
Completeness to θ = 30.74°	9800%
Refinement method	Full-matrix least-squares on F^2
Data / restraints / parameters	328 / 1 / 14
Goodness-of-fit	2.12
Final R indices [I>2σ(I)]	R_{obs} = 0.0200, wR_{obs} = 0.0536
R indices [all data]	R_{all} = 0.0200, wR_{all} = 0.0536
Extinction coefficient	?
Largest diff. peak and hole	0.40 and -0.82 $e \cdot Å^{-3}$

$R = \Sigma||F_o|-|F_c|| / \Sigma|F_o|$, $wR = \{\Sigma[w(|F_o|^2 - |F_c|^2)^2] / \Sigma[w(|F_o|^4)]\}^{1/2}$ and $w=1/(\sigma^2(I)+0.0004I^2)$

Table 19. Bond angles [°] for $MAGeI_3$ at 293 K with estimated standard deviations in parentheses.

Label	Angles
I-Ge-I’	96.98(4)

Table 20. Atomic coordinates ($x10^4$) and equivalent isotropic displacement parameters ($Å^2x10^3$) for $MAGeI_3$ at 293 K with estimated standard deviations in parentheses.

Label	x	y	z	Occupancy	U_{eq}*
I	0.3237(1)	0.1619(1)	0.2509(1)	1	0.060(1)
Ge	0.0000	0.0000	0.1259(2)	1	0.031(1)
N	0.0000	0.0000	0.6490(40)	1	0.216(11)
C	0.0000	0.0000	0.5150(40)	1	0.216(11)

*U_{eq} is defined as one third of the trace of the orthogonalized U_{ij} tensor.

4.3 optical characterization of Hybrid Germanium Iodide Perovskites

UV/Vis Absorption Spectroscopy

The crystals formed using technique one was used for visual characterization of the perovskites. The perovskite crystalline powders for the homologous series absorb light in the visible portion of the spectrum with most of the compounds being red in color. In order to accurately determine the optical bandgaps, diffuse reflectance measurements were performed using the Kubelka-Munk equation to convert reflectance into absorbance: [41]

$$\frac{K}{s} = \frac{(1 - R_\infty)^2}{2R_\infty}$$

Where, K=absorption coefficient, K=$\frac{4\pi\kappa}{\lambda}$

R= diffuse reflectance

S=scattering coefficient

The energy gap of the perovskites, and hence the wavelength at which they absorb, and thus the color of the samples, may then be determined using the equation $E(ev) = \frac{1240}{\lambda(nm)}$ and the diagrams.

$(BA)_2GeI_4$ (n = 1)

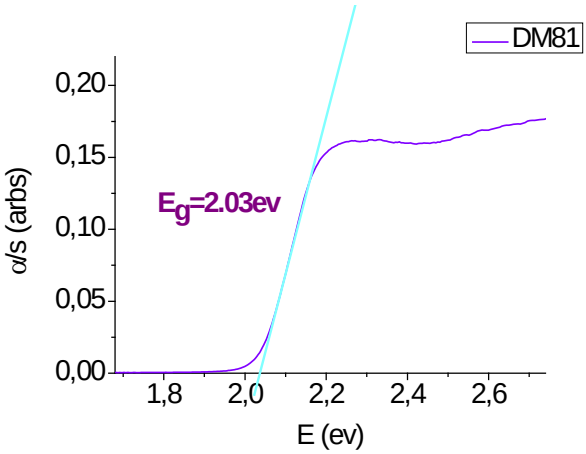

$\lambda(nm) = \frac{1240}{E(ev)} = \frac{1240}{2.03}$=*610.8nm* ***orange***

Figure 14. Absorption spectra (left) and a photograph of the as prepared sample (right) for BA_2GeI_4.

The absorption of the BA_2GeI_4 perovskite (n = 1) is shown in **Figure 14**. The band gap for this compound is estimated at E_g = 2 eV, in agreement with the orange color of the thin rod-shaped crystals.

$(BA)_2(MA)Ge_2I_7$ (n = 2)

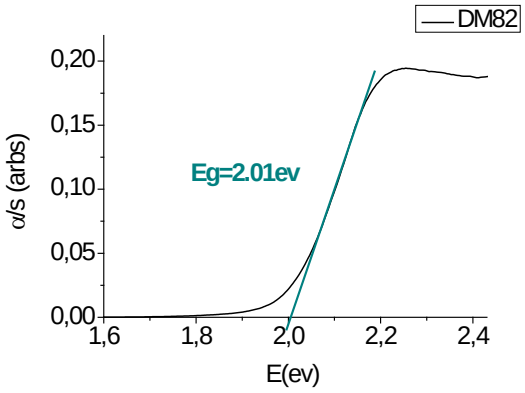

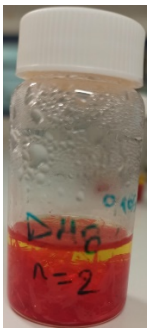

$$\lambda(nm) = \frac{1240}{E(ev)} = \frac{1240}{2.01} = 616.9nm$$ **Orange**

Figure 15. Absorption spectra (left) and a photograph of the as prepared sample (right) for $BA_2(MA)Ge_2I_7$.

The absorption of the $BA_2(MA)Ge_2I_7$ perovskite (n = 2) is shown in **Figure 15**. The band gap for this compound is estimated at E_g = 2 eV, in agreement with the orange color of the thin rod-shaped crystals of n = 1. As a result, we can report that the desired compound was not synthesized successfully at this stage of the ongoing work.

$(BA)_2(MA)_2Ge_3I_{10}$ (n = 3)

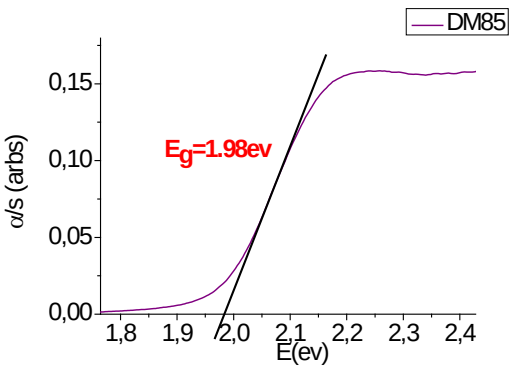

$$\lambda(nm) = \frac{1240}{E(ev)} = \frac{1240}{1.98}$$=626.3nm ***Red***

Figure 16. Absorption spectra (left) and a photograph of the as prepared sample (right) for $BA_2(MA)_2Ge_3I_{10}$.

The absorption of the $BA_2(MA)_2Ge_3I_{10}$ perovskite (n = 3) is shown in **Figure 16**. The band gap for this compound is estimated at E_g = 2 eV, in agreement with the orange color of the thin rod-shaped crystals of n = 1. As a result, we can report that the desired compound was not synthesized successfully at this stage of the ongoing work.

$(BA)_2(MA)_3Ge_4I_{13}$ (n = 4)

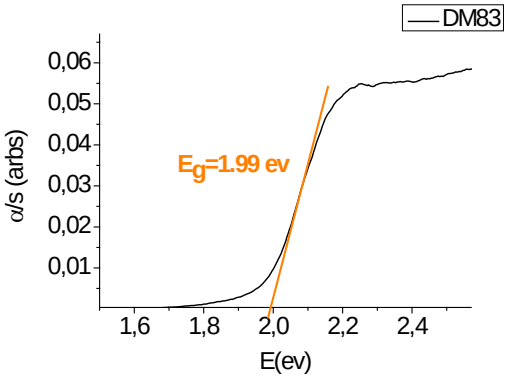

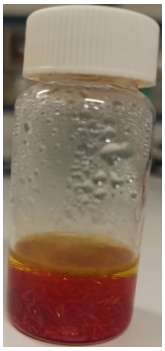

$$\lambda(nm) = \frac{1240}{E(ev)} = \frac{1240}{1.99} = 623.1nm$$

Orange ***Red***

Figure 17. Absorption spectra (left) and a photograph of the as prepared sample (right) for $BA_2(MA)_3Ge_4I_{13}$.

The absorption of the $BA_2(MA)_3Ge_4I_{13}$ perovskite (n = 4) is shown in **Figure 17**. The band gap for this compound is estimated at E_g = 2 eV, in agreement with the orange color of the thin rod-shaped crystals of n = 1. As a result, we can report that the desired compound was not synthesized successfully at this stage of the ongoing work.

$MAGeI_3$ (n =∞)

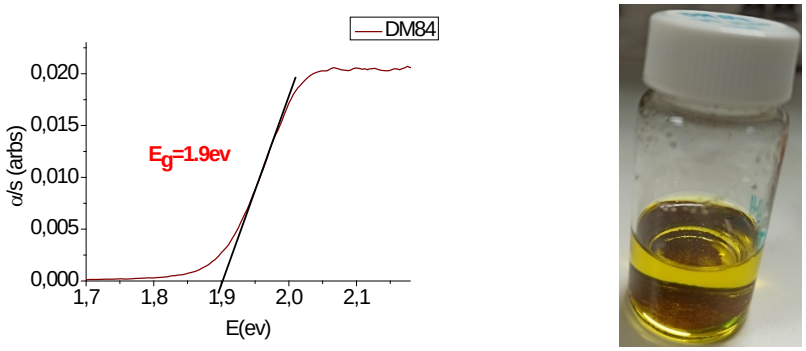

$$\lambda(\text{nm}) = \frac{1240}{\text{E(ev)}} = \frac{1240}{1.9} = 652.6\text{nm}$$ **Red**

Figure 18. Absorption spectra (left) and a photograph of the as prepared sample (right) for $MAGeI_3$.

The absorption of the MAGeI perovskite (n = ∞) is shown in **Figure 18**. The band gap for this compound is estimated at E_g = 1.9 eV, in agreement with the dark red color of the thin rod-shaped crystals of n = ∞. As a result, we can report that the desired compound was synthesized successfully.

5. Conclusions

The study of the homologous series of the 2D dimensional germanium perovskites $CH_3(CH_2)_3NH_3)_2$ $(CH_3NH_3)_{(n-1)}$ $Ge_nI_{(3n+1)}$ is reported here for the first time. In the context of the present study, we have been successful in determining the crystal structures of the materials up to the n = 4 member of the family via a series of trial-and-error experiments on the synthetic procedure. We have encountered several difficulties, however, in the synthesis and particularly in the isolation of the desired compounds in their pure form, due to the air instability of the compounds that do not allow a proper characterization of the physical and chemical properties of the bulk materials. Thus, only the perovskites with n = 1 and n = ∞ could be obtained in pure form, whereas the intermediate family members have not been obtained in a pure form so far. The future goal of this project is to isolate in pure phase the 2D germanium perovskites for all n (n = 1-5) by eliminating the oxidized material from the reaction mixtures. Once this is achieved, we will be able to study these materials for various energy applications, being environmentally friendly due to the low toxicity of germanium. Work in progress suggest that this feature is possible by careful modification of the reaction conditions.

6. References

1. Tilley, R. J. D. *Perovskites: Structure-Property Relationships*. (John Wiley & Sons, Ltd, 2016). doi:10.1002/9781118935651.

2. Chen, S.L., Shang, Y., He, C.T. et al. (2018). *CrystEngComm* 20: 7458.

3. Emmanouil Spanakis: EXPERIMENT P2-MADE INSULATION WITH LIQUID CHEMICAL METHOD, Laboratory of Solid Materials, Department of Materials Science and Technology - University of Crete.

4. Burschka, J.; Pellet, N.; Moon, S. J.; Humphry-Baker, R.; Gao, P.; Nazeeruddin, M. K.; Gratzel, M. Sequential Deposition as a Route to High-Performance Perovskite-Sensitized Solar Cells. Nature 2013, 499, 316−319.

5. Jeon, N. J.; Noh, J. H.; Kim, Y. C.; Yang, W. S.; Ryu, S.; Il Seok, S. Solvent Engineering for High-Performance Inorganic-Organic Hybrid Perovskite Solar Cells. Nat. Mater. 2014, 13, 897−903.

6. Boix, P. P.; Agarwala, S.; Koh, T. M.; Mathews, N.; Mhaisalkar, S. G. Perovskite Solar Cells: Beyond Methylammonium Lead Iodide. J. Phys. Chem. Lett. 2015, 6, 898−907.

7. Gao, P.; Gratzel, M.; Nazeeruddin, M. K. Organohalide Lead Perovskites for Photovoltaic Applications. Energy Environ. Sci. 2014, 7, 2448−2463.

8. De Angelis, F. Modeling Materials and Processes in Hybrid/ Organic Photovoltaics: From Dye-Sensitized to Perovskite Solar Cells. Acc. Chem. Res. 2014, 47, 3349−3360.

9. Green, M. A.; Ho-Baillie, A.; Snaith, H. J. The Emergence of Perovskite Solar Cells. Nat. Photonics 2014, 8, 506−514.

10. Miyasaka, T. Perovskite Photovoltaics: Rare Functions of Organo Lead Halide in Solar Cells and Optoelectronic Devices. Chem. Lett. 2015, 44, 720−729.

11. Stoumpos, C. C.; Kanatzidis, M. G. The Renaissance of Halide Perovskites and Their Evolution as Emerging Semiconductors. Acc. Chem. Res. 2015, 48, 2791−802.

12. Jung, H. S.; Park, N.-G. Perovskite Solar Cells: From Materials to Devices. Small 2015, 11, 10−25.

13. Etgar, L.; Gao, P.; Xue, Z.; Peng, Q.; Chandiran, A. K.; Liu, B.; Nazeeruddin, M. K.; Grätzel, M. Mesoscopic CH3NH3PbI3/TiO2 Heterojunction Solar Cells. J. Am. Chem. Soc. 2012, 134, 17396−17399.

14. Lee, M. M.; Teuscher, J.; Miyasaka, T.; Murakami, T. N.; Snaith, H. J. Efficient Hybrid Solar Cells Based on Meso-Superstructured Organometal Halide Perovskites. Science 2012, 338, 643−647.

15. Kim, H.-S.; Lee, C.-R.; Im, J.-H.; Lee, K.-B.; Moehl, T.; Marchioro, A.; Moon, S.-J.; Humphry-Baker, R.; Yum, J.-H.; Moser, J. E.; Grätzel, M.; Park, N.-G. Lead Iodide Perovskite Sensitized All-Solid-State Submicron Thin Film Mesoscopic Solar Cell with Efficiency Exceeding 9%. Sci. Rep. 2012, 2, 591.

16. Fabini, D. Quantifying the Potential for Lead Pollution from Halide Perovskite Photovoltaics. J. Phys. Chem. Lett. 2015, 6, 3546− 3548.

17. Niu, G.; Guo, X.; Wang, L. Review of Recent Progress in Chemical Stability of Perovskite Solar Cells. J. Mater. Chem. A 2015, 3, 8970− 8980.

18. Hao, F.; Stoumpos, C. C.; Cao, D. H.; Chang, R. P. H.; Kanatzidis, M. G. Lead-Free Solid-State Organic-Inorganic Halide Perovskite Solar Cells. Nat. Photonics 2014, 8, 489−494.

19. Noel, N. K.; Stranks, S. D.; Abate, A.; Wehrenfennig, C.; Guarnera, S.; Haghighirad, A.; Sadhanala, A.; Eperon, G. E.; Pathak, S. K.; Johnston, M. B.; Petrozza, A. M.; Herz, L. M.; Snaith, H. J. Lead-Free Organic-Inorganic Tin Halide Perovskites for Photovoltaic Applications. Energy Environ. Sci. 2014, 7, 3061−3068.

20. Ogomi, Y.; Morita, A.; Tsukamoto, S.; Saitho, T.; Fujikawa, N.; Shen, Q.; Toyoda, T.; Yoshino, K.; Pandey, S. S.; Ma, T.; Hayase, S. CH3NH3SnxPb(1-x)I3 Perovskite Solar Cells Covering up to 1060 nm. J. Phys. Chem. Lett. 2014, 5, 1004−1011.

21. Zuo, F.; Williams, S. T.; Liang, P.-W.; Chueh, C.-C.; Liao, C.-Y.; Jen, A. K. Y. Binary-Metal Perovskites Toward High-Performance Planar-Heterojunction Hybrid Solar Cells. Adv. Mater. 2014, 26, 6454− 6460.

22. Hao, F.; Stoumpos, C. C.; Chang, R. P.; Kanatzidis, M. G. Anomalous Band Gap Behavior in Mixed Sn and Pb Perovskites Enables Broadening of Absorption Spectrum in Solar Cells. J. Am. Chem. Soc. 2014, 136, 8094−8099.

23. Hao, F.; Stoumpos, C. C.; Guo, P.; Zhou, N.; Marks, T. J.; Chang, R. P. H.; Kanatzidis, M. G. Solvent-Mediated Crystallization of CH3NH3SnI3 Films for Heterojunction Depleted Perovskite Solar Cells. J. Am. Chem. Soc. 2015, 137, 11445−11452.

24. Smith, I. C.; Hoke, E. T.; Solis-Ibarra, D.; McGehee, M. D.; Karunadasa, H. I. A Layered Hybrid Perovskite Solar-Cell Absorber with Enhanced Moisture Stability. Angew. Chem., Int. Ed. 2014, 53, 11232− 11235.

25. Cao, D. H.; Stoumpos, C. C.; Farha, O. K.; Hupp, J. T.; Kanatzidis, M. G. 2D Homologous Perovskites as Light-Absorbing Materials for Solar Cell Applications. J. Am. Chem. Soc. 2015, 137, 7843−7850.

26. Stoumpos, C. C. *et al*. Hybrid Germanium Iodide Perovskite Semiconductors: Active Lone Pairs, Structural Distortions, Direct and Indirect Energy Gaps, and Strong Nonlinear Optical Properties. *J. Am. Chem. Soc.* **137**, 6804–6819 (2015).

27. Dmitriev, V. G., Gurzadyan, G. G., Nikogosyan, D. N. Handbook of Nonlinear Optical Crystals; 3rd rev. ed.; Springer-Verlag: Heidelberg, 1999; Vol. 64.

28. Fox, M. *Optical properties of solids*. (Oxford University Press, 2010).

29. Calabrese, J.; Jones, N. L.; Harlow, R. L.; Herron, N.; Thorn, D. L.; Wang, Y. Preparation and Characterization of Layered Lead Halide Compounds. J. Am. Chem. Soc. 1991, 113, 2328−2330.

30. Kataoka, T.; Kondo, T.; Ito, R.; Sasaki, S.; Uchida, K.; Miura, N. Magneto-Optical Study on Excitonic Spectra in (C6H13NH3)2PbI4. Phys. Rev. B: Condens. Matter Mater. Phys. 1993, 47, 2010−2018.

31. Muljarov, E. A.; Tikhodeev, S. G.; Gippius, N. A.; Ishihara, T. Excitons in Self-Organized Semiconductor-Insulator Superlattices – PbIBased Perovskite Compounds. Phys. Rev. B: Condens. Matter Mater. Phys. 1995, 51, 14370−14378.

32. Ishihara, T.; Takahashi, J.; Goto, T. Exciton-State in Two- Dimensional Perovskite Semiconductor (C10H21NH3)2PbI4. Solid State Commun. 1989, 69, 933−936.

33. Kagan, C. R.; Mitzi, D. B.; Dimitrakopoulos, C. D. Organic- Inorganic Hybrid Materials as Semiconducting Channels in Thin-Film Field-Effect Transistors. Science 1999, 286, 945−947.

34. Shibuya, K.; Koshimizu, M.; Takeoka, Y.; Asai, K. Scintillation Properties of (C6H13NH3)2PbI4: Exciton Luminescence of an Organic/ Inorganic Multiple Quantum Well Structure Compound Induced by 2.0 MeV Protons. Nucl. Instrum. Methods Phys. Res., Sect. B 2002, 194, 207− 212.

35. Stoumpos, C. C.; Soe, C. M. M.; Tsai, H.; Nie, W.; Blancon, J.- C.; Cao, D. H.; Liu, F.; Traoré, B.; Katan, C.; Even, J.; Mohite, A. D.; Kanatzidis, M. G. Chem. 2017, 2, 427−440.

36. Stoumpos, C. C.; Cao, D. H.; Clark, D. J.; Young, J.; Rondinelli, J. M.; Jang, J. I.; Hupp, J. T.; Kanatzidis, M. G. Chem. Mater. 2016, 28, 2852−2867.

37. Stoumpos, C. C.; Mao, L.; Malliakas, C. D.; Kanatzidis, M. G. Inorg. Chem. 2017, 56, 56−73.

38. Mitzi, D. B.; Feild, C. A.; Harrison, W. T. A.; Guloy, A. M. Nature 1994, 369, 467−469.

39. Mitzi, D. B. Synthesis, Crystal Structure, and Optical and Thermal Properties of $(C_4H_9NH_3)_2MI_4$ (M = Ge, Sn, Pb). *Chem. Mater.* **8**, 791–800 (1996).

40. Emmanouil Spanakis: EXPERIMENT X2: STRUCTURAL AND DIELECTRIC CHARACTERISTICS OF INSULATOR, Laboratory of Solid Materials, Department of Materials Science and Technology - University of Crete.

41. Kubelka-Munk: Solutions in Optical Spectroscopy